Investigations of radiation pressure : optical side-band cooling of a trampoline resonator and the effect of superconductivity on the Casimir force

Eerkens, H.J.

4

Exploring Nested Resonators for Optomechanical Cooling

Optomechanical systems have gained increasing popularity over the past years for their promising possibilities to explore quantum mechanical behaviour in macroscopic objects. By coupling an optical field to a mechanical resonator, it may be possible to transfer the quantum mechanical properties of the photons to massive objects. This process is counteracted by influences from the outside world and by the thermal occupancy of the mechanical resonator. It is therefore beneficial to operate the resonator close to its quantum mechanical ground state. Several systems involving a mechanical mode with a relatively high resonance frequency have already been cooled to a phonon occupation less than one [26–30]. For lower frequency resonators the effective temperature associated with the quantum ground state lies lower, increasing the need for cryostats with lower base temperature. Since the base temperature of cryostats is limited in practice, optical side-band cooling is needed to reach lower effective mode temperatures. A higher possible optical cooling factor lowers the demand for the cryostat base temperature. In addition, low frequency resonators are more sensitive to surrounding vibrational noise. This means that the system should mechanically be better isolated from the environment.

In this chapter we will show mechanical isolation of a trampoline resonator in the form of a second resonator acting as a mechanical low-pass filter. Although this outer resonator successfully isolates the inner resonator from mechanical vibrations, its motion also influences the optomechanical response of the system.

This chapter is partially based on: M. J. Weaver, B. Pepper, F. M. Buters, H. J. Eerkens, G. Welker, B. Perock, K. Heeck, S. de Man, and D. Bouwmeester, "Nested trampoline resonators for optomechanics," *Appl. Phys. Lett.*, **108**, 033501, (2016).

4.1 Optomechanical cooling

In chapter 2 we presented optical cooling of a low frequency mechanical resonator [72]. Using a two laser scheme operating at different frequencies, it was possible to reach an effective temperature of $4\,\mathrm{K}$ starting from room temperature. Lower effective temperatures could not be detected due to mechanical noise in our system. This is visualized in Figure 4.1, which shows the mechanical power spectral density of a cooled resonator buried under mechanical noise peaks. This puts a limit on the observable cooling factor and therefore on the lowest effective temperature that can be measured when the optical cooling is started from a certain base temperature.

The possible cooling factor and the effect of the mechanical noise peaks depends on the intrinsic quality factor of the resonator. When the intrinsic linewidth is smaller, it can be damped more until it disappears in the background. Since the single resonators are dominated by clamping losses [85], a high quality factor cannot be guaranteed. Not only can it change every time a sample is remounted, it may also change drastically when the resonator is cooled in a cryostat.

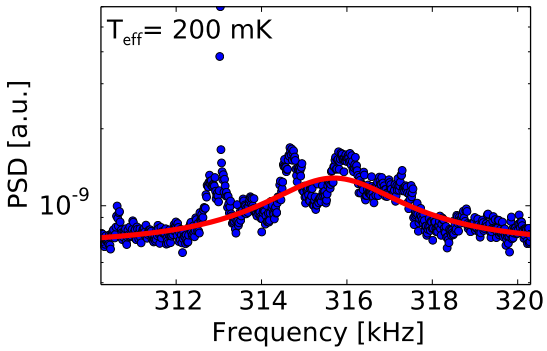

Figure 4.1: Power spectral density of a single resonator cooled to an effective temperature of $200\,\mathrm{mK}$, the Lorentzian peak describing the mechanical motion is buried under mechanical noise peaks.

The exact source of the mechanical noise peaks is unknown, but it is likely that they originate from the multiple components of our set-up. With a cavity length of $5\,\mathrm{cm}$ it is difficult to create a monolithic system that is less prone to internal vibrations. We therefore need to isolate the trampoline resonator from the vibrations of the set-up and the cryostat. Since the noise may arise from anywhere in the set-up, we designed an on-chip isolation to be as close to the resonator as possible. An extra low frequency resonator is fabricated around the inner resonator and acts as a low-pass filter [86–90]. An optical image of this nested resonator is shown in Figure 4.2(a). The inner resonator has a mirror diameter of $80\,\mu\mathrm{m}$ and a resonance frequency of $240\,\mathrm{kHz}$. The outer resonator consists of a ring of $500\,\mu\mathrm{m}$ thick silicon hanging from four Si_3N_4 arms. Due to the relatively large mass it has a resonance frequency of $2.4\,\mathrm{kHz}$. A description of the fabrication process is given in [91].

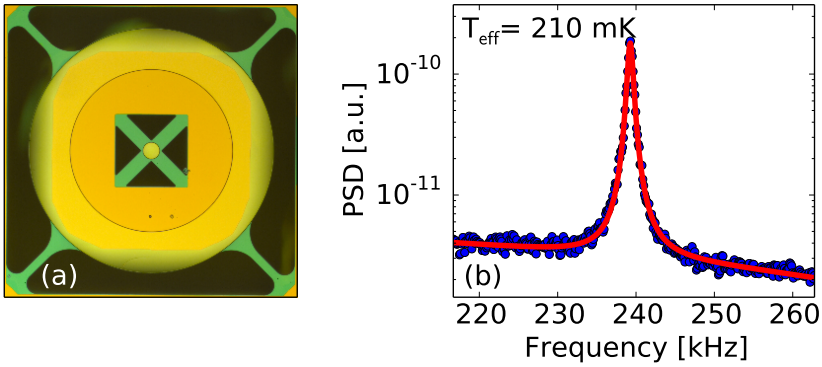

Figure 4.2: Nested resonators: (a) Optical image of a nested resonator consisting of an inner resonator with mirror diameter of $80\,\mu$m and resonance frequency $240\,$kHz and an outer resonator with resonance frequency $2.4\,$kHz; (b) Power spectral density of the motion of the inner resonator cooled to an effective temperature of $210\,$mK, the mechanical noise peaks are no longer visible.

To check the influence of clamping on the quality factor, the sample was mounted and remounted several times while the quality factor of both the inner and outer resonator was measured. For the outer resonator values changed by an order of magnitude, while the inner resonator quality factors varied less than ten percent [91]. So the outer resonator guarantees a consistent good quality factor of the inner resonator.

Optical cooling of the inner resonator was performed next to check the isolation provided by the outer resonator. Using the set-up described in chapter 2, the pump laser was fixed at a detuning of $\Delta = -\frac{1}{2}\Omega_{\mathrm{m}}$ with respect to the cavity resonance. The laser power was then increased in steps while at each step the mode temperature was determined from the area under the mechanical power spectral density. At an effective temperature of $210\,$mK, the resonator is still clearly distinguishable and no other noise peaks are visible, see Figure 4.2(b). The outer resonator successfully isolates the inner resonator from mechanical noise, which means that we are able to detect lower effective temperatures than with a single resonator.

We increase the laser power even further to find the lowest effective temperature we can reach. The effective mode temperature as a function of pump laser power is shown in Figure 4.3(a). The effective temperature is linear in laser power, showing that we are not yet limited by phase noise in our cavity light [65]. The lowest mode temperature that could be determined is $23\,$mK. Starting from room temperature, this means a cooling power factor of 13.000. Note again that the power spectral densities in Figure 4.3(b), taken at different laser powers, show no influence of mechanical noise, even at the lowest effective temperatures. Further cooling is limited by the intrinsic linewidth of the resonator and by the stability of the system. The resonance at $23\,$mK is barely distinguishable from the background. Further remarks on the system stability shall be given in the following sections. Still, a cooling factor of 13.000

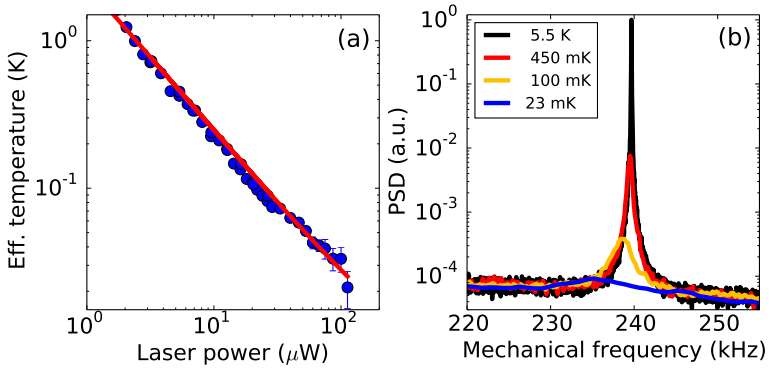

Figure 4.3: Optical cooling of a nested trampoline resonator from room temperature: (a) Effective mode temperature of the inner resonator as a function of pump laser power, a mode temperature of 23 mK is reached; (b) Power spectral densities at several effective temperatures, even at 23 mK the motion of the inner resonator can be clearly distinguished.

means that ground state cooling should be possible starting from a base temperature of 100 mK. This is an easily achievable temperature for a dilution refrigerator.

4.2 Influence of the outer resonator motion

Adding an outer resonator solves several problems, but the mechanical properties of this extra resonator also influence the cavity length and therefore also couple to the optical field. To investigate the effect of the outer resonator, we performed a sweep of the pump laser detuning with respect to the cavity resonance. The detuning was altered in steps of 5 kHz and at each step the mechanical spectrum of the inner resonator was recorded. From each spectrum we determined three parameters, the effective damping, frequency shift and effective temperature. The dependence of these parameters on the pump laser detuning is shown in Figure 4.4. The red line through the data shows a fit to the optomechanics theory. From the fits we could determine an intracavity power of $3.01 \pm 0.04\,\mu$W and a cavity linewidth of $\kappa = 52 \pm 1$ kHz. This parameter coincides well with the previously determined value of $\kappa = 53$ kHz obtained from an optical cavity ring-down.

The theory fits well to the data, so it seems that the effect of the outer resonator is indeed minimal. However, when a detuning of $\Delta = -\frac{1}{2}\Omega_\mathrm{m}$ is reached, the system becomes unstable and the laser locks, on which our measurement scheme depends, can no longer longer follow the cavity length changes. The value of Δ where this effect occurs is not fixed, but depends on laser power and happens sooner with higher laser power. Therefore the system also becomes unstable when the detuning is fixed at $\Delta = -\Omega_\mathrm{m}$ and the power is increased. To fully understand this effect and the influence of the outer resonator on the system, we need to look at the schematic shown in Figure 4.5. The masses of the mirror and the silicon ring of the outer resonator are

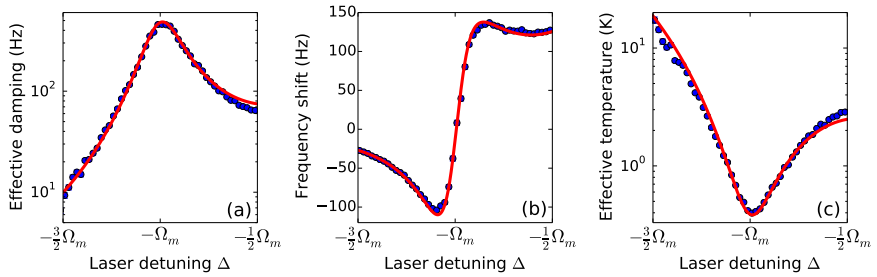

Figure 4.4: Sweep of the pump laser detuning with respect to the cavity resonance and the response of the mechanical motion of the inner resonator: (a) Effective damping; (b) frequency shift and (c) effective temperature. The blue dots show data, the red line is a fit with theory.

indicated, as well as the optical field and the big mirror at the opposite end of the cavity. The Si_3N_4 arms of both resonators are represented as a spring parallel to a damper.

The optical field interacts directly with the inner resonator. However, at frequencies below the resonance of the outer resonator, the transfer of motion between the two resonators is equal to one. This means that the resonators effectively move as a single resonator and the optical field interacts with the outer resonator as well. For clarity, we will separate the optomechanical response into two frequency ranges. For the high frequency range, the outer resonator hardly moves and the optical field only couples to the inner resonator motion. The ratio between the cavity linewidth and the mechanical frequency makes the optomechanical interaction side-band resolved, which means large optical damping and relatively small optical spring effect when the laser is detuned at $\Delta = -\Omega_\mathrm{m}$. At low frequencies, the optical field couples effectively to both resonators, but due to a different mechanical frequency to cavity linewidth ratio, this interaction is not side-band resolved. The result is a relatively low damping effect and a large optical spring. The spring effect drives the mechanical frequency of the outer resonator down, which increases the sensitivity for low frequency noise and makes the system unstable.

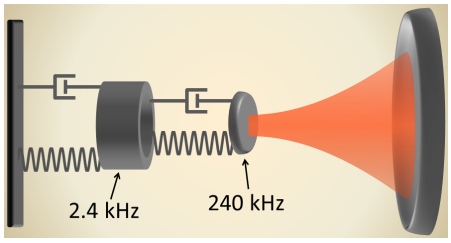

Figure 4.5: Schematic of the inner and outer resonator coupled to an optical field. The Si_3N_4 arms can be represented as a spring and a damper, with the masses coming from the mirror and the silicon ring.

Note that at positive detunings, the optical spring effect drives the resonator towards higher frequencies. The static response of the system decreases, which increases the possibility to measure at positive detunings. This is almost not possible for single resonators. Since we are ultimately only interested in cooling the outer resonator, we have not investigated this effect further.

4.3 Damping of outer resonator motion

The stability of the system is also influenced by the amplitude of the outer resonator motion. The outer resonator has a mode mass of $m_{\text{eff}} = 160 \times 10^{-9}$ kg and a resonance frequency of $\Omega_m/2\pi = 2.4$ kHz, which means that at room temperature it has an RMS motion of

$$x_{\text{rms}} = \sqrt{\langle x^2 \rangle} = \sqrt{\frac{k_B T}{m_{\text{eff}} \Omega_m^2}} = 10.6\,\text{pm}, \tag{4.1}$$

where k_B is the Boltzmann constant. Compared to the cavity length of $L = 5$ cm, the change of the cavity resonance frequency at 2.4 kHz is

$$\Delta\omega_{cav} = \omega_{cav} \frac{\Delta L}{L} = 2\pi \times 59.2\,\text{kHz}. \tag{4.2}$$

This is not a significant portion of the range of 16 MHz of our Pound-Drever-Hall (PDH) cavity frequency lock [64, 72]. But under the influence of external vibrations the outer resonator can easily be driven to an amplitude of several nanometers, beyond the reach of the lock. One solution is to prevent these vibrations, but since they can come from within the set-up, this may require yet another on-chip resonator.

It is clear that the motion of the outer resonator needs to be controlled. Since reading out the motion via the intracavity light might interfere with the already existing PDH lock, we have chosen to read out the motion using fiber interferometry [92]. A cleaved single mode fiber end is positioned behind the cavity at a distance of several hundred micrometers from the outer resonator. Light from a telecom laser ($\lambda = 1550$ nm) travels via a fiber coupler to the cleaved fiber end. The light reflected at the outer resonator surface couples back into the fiber and passes the fiber coupler again. It exits the coupler via a different portal than where the laser light originally entered and falls onto a detector. The resonator motion translates linearly to detector signal when the laser frequency is tuned at quadrature. The sensitivity of the readout in Volts per meter can be determined from a single laser frequency scan at the start of each measurement [92]. We can therefore directly determine the resonator motion in meters.

To control the motion, we need to apply a force. There are many ways to do this, but we have chosen to investigate two different methods, which will be described and compared in this section. First we made the outer resonator one half of a parallel-plate capacitor, by coating it with a conductive aluminium layer. The other half of the capacitor is created by positioning an aluminium coated plate in its vicinity. The capacitative energy causes an electrostatic force that can be adjusted by setting the voltage across the two surfaces.

Another method to influence the resonator motion is by applying an electrostatic field gradient around the resonator [93]. This is achieved by positioning a small wire near the resonator and setting its potential with respect to the sample mount. The dielectric material of the outer resonator (silicon) polarizes in this electrostatic field and is pulled towards the wire. We are able to drive or damp the motion, depending on the phase of the feedback signal compared to the motion of the resonator.

4.3.1 Capacitative control of the resonator motion

A capacitor consists of two parallel conductive plates close together. The energy stored in the electric field between the two plates is given by

$$E = \frac{1}{2}CV^2, \tag{4.3}$$

with V the voltage across the capacitor and C the capacitance, which is equal to $C = \frac{\varepsilon A}{d}$. Here ε is the electric permittivity of the material between the plates (in our set-up this is usually vacuum or air, so we can take $\varepsilon = \varepsilon_0$), A is the overlap area and d is the distance between the plates (both unknown in our set-up). When one of the plates is free to move, the distance changes and therefore the capacitance. The force experienced by the movable plate is given by

$$F_c = -\frac{1}{2}\frac{\partial C}{\partial d}V^2 = \frac{\varepsilon_0 A V^2}{2d^2}. \tag{4.4}$$

This force can be used to control the motion of the outer resonator, when it is part of a parallel plate capacitor. Since the resonator is originally not made of conductive materials, it is coated with a conductive layer of aluminium. A second silicon wafer, pressed against the sample wafer and also coated with aluminium, serves as the second capacitor plate. If we would press the two wafers directly on top of each other, the aluminium coating would make contact, thereby eliminating the capacitance. So part of the wafer is recessed prior to coating, and the recessed part is aligned to the outer resonator. A schematic of the sample package is shown in Figure 4.6. To allow optical access for the fiber interferometric read-out, a hole is etched in the center of the recessed area. Since we are only interested in the general behaviour of this sample, we have performed the measurements at room temperature and ambient pressure without any vibration isolation.

To control the motion of the outer resonator, we apply a voltage across the two coated surfaces via wires attached at the edge of the wafers[1]. Since the force depends quadratically on the voltage, it is always attractive. Applying a DC voltage would only pull on the resonator and an AC voltage would result in a force at twice the chosen frequency. When the applied voltage is a sum of these voltages, $V = V_{\mathrm{DC}} + V_{\mathrm{AC}}\cos(\omega t)$, the force on the resonator contains a cross-term that is linear in V_{DC} and at the same frequency as the applied AC voltage:

$$F_c = \frac{\varepsilon_0 A}{2d^2}\left[\left(V_{\mathrm{DC}}^2 + \frac{1}{2}V_{\mathrm{AC}}^2\right) + 2V_{\mathrm{DC}}V_{\mathrm{AC}}\cos(\omega t) + \frac{1}{2}V_{\mathrm{AC}}^2\cos(2\omega t)\right]. \tag{4.5}$$

[1] Only the recessed part of the silicon wafer was electrically connected.

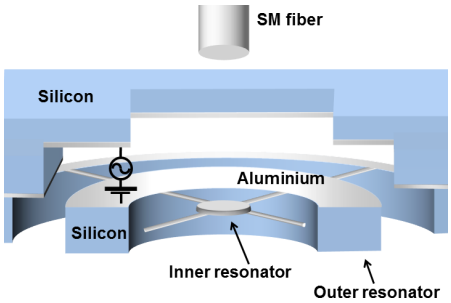

Figure 4.6: Schematic of the sample package allowing capacitative control of the outer resonator. The nested resonator is coated with a conductive aluminium layer. An aluminium coated silicon wafer is pressed against the resonator wafer. Part of the silicon wafer is recessed to prevent direct contact between the coating layers. A single mode (SM) fiber and hole for optical access are also indicated.

We verify whether this force can indeed be used to drive the outer resonator by looking at the response of the system to the 1f-component of the force, the second term on the RHS in Eq. 4.5. The DC voltage and the amplitude of the AC voltage are both set to 1 V, while the frequency of the AC voltage is scanned across the resonance frequency of 940 Hz. The signal from the fiber interferometer at each frequency step is detected and demodulated by a lock-in amplifier. The signal can be converted to nanometers by a separately performed calibration of the interferometer signal. The result is shown in Figure 4.7. For comparison the red line in the same figure shows the thermal motion of the resonator at room temperature obtained from a Fourier transform of the detector signal without drive.

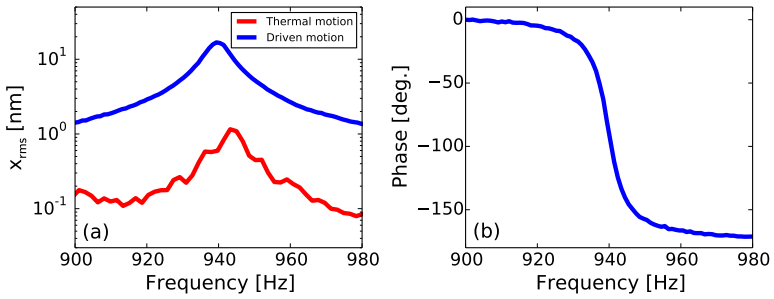

Figure 4.7: Frequency scan of the response of the outer resonator to the capacitative force: (a) Amplitude of the resonator motion (blue line) compared to the undriven thermal motion (red line); (b) Phase of the driven resonator motion.

It is clear that the capacitative drive of the outer resonator works and can easily increase the resonator motion by more than an order of magnitude. So it should in principle be possible to create a feedback loop to damp the motion, instead of

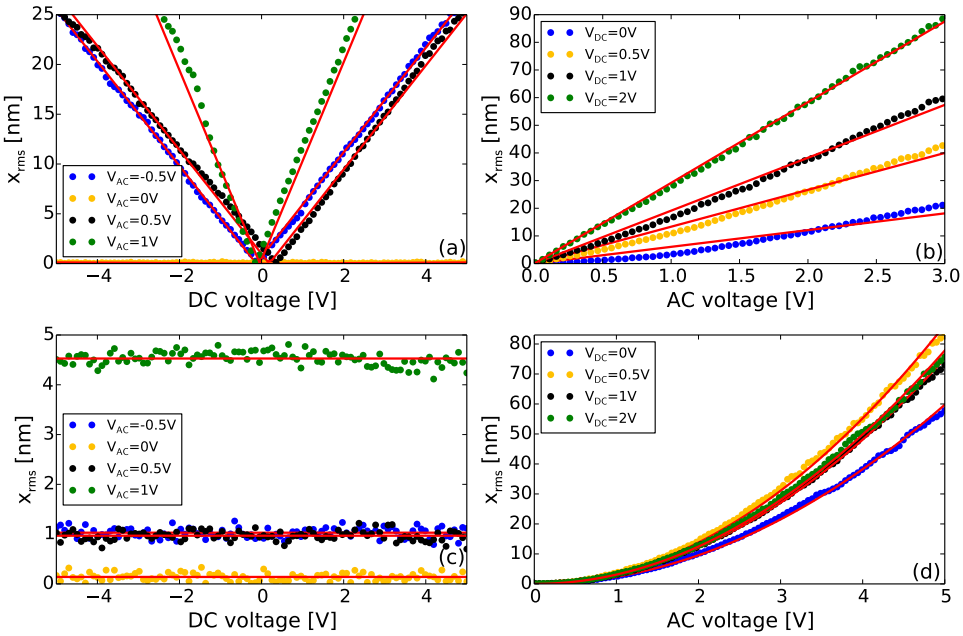

Figure 4.8: Scans of the (a,c) DC and (b,d) AC voltage while monitoring the response (a,b) at the applied frequency and (c,d) at twice the applied frequency. The points show data while the red lines show fits of the expected response.

driving it. But before we investigate this further, we want to be sure that the system responds as expected. We therefore performed sweeps of the DC and AC voltages while monitoring the 1f- and 2f-components of the force response (the second and third terms in Equation 4.5 respectively).

When the AC voltage is applied at the resonance frequency, with the signal demodulated at the same frequency, the response should be linear in both V_{AC} and V_{DC}. Figures 4.8(a) and 4.8(b) demonstrate indeed roughly a linear increase in resonator motion. Note that since we measure the RMS motion, the response is also positive at negative voltages.

When we apply the AC voltage at half the resonance frequency, we still expect response at the resonance frequency due to the third term in Equation 4.5. This term is independent of the DC voltage, as indeed shown in Figure 4.8(c). The average RMS motion increases with AC voltage, which we expect, and Figure 4.8(d) shows that this response is indeed quadratic.

In general, the voltage sweep show the expected trends. However, the linear response shows some small deviations. Figure 4.8(a) shows a tiny offset in DC voltage where the response is minimal, which should be at zero voltage. This is due to a small background voltage caused by a difference in work function between the two aluminium coatings.

A closer look at the linear response in Figure 4.8(b) shows some nonlinear be-

haviour. This deviation may be caused by measurement imprecisions, but it is also likely that other aluminium coated areas in the vicinity of the outer resonator form stray capacitors, which influence the resonator response.

Preventing the formation of stray capacitors is challenging, since it depends on a combination of sample fabrication techniques and manually aligning the two wafers. Minimizing the effect of unwanted capacitors generally also lowers the capacitance used to control the outer resonator. The aligning process is already quite cumbersome and requires a sample mount flexible enough for manipulation while being able to fix the wafers when aligned. Another disadvantage of the capacitative drive is that coating the nested resonator with a conductive aluminium layer is likely to negatively affect the mechanical quality factor of the inner resonator. So investigating another method for controlling the outer resonator motion seems beneficial.

But before we completely switch to another method, we use the constructed sample to demonstrate the amount of mechanical isolation it provides. The amount of isolation is proportional to the transferred energy, which again is proportional to the squared amplitude of the outer resonator motion [94], which we can measure directly. We drive the outer resonator capacitatively with a DC voltage of $-2\,\mathrm{V}$ and an AC voltage amplitude of $1\,\mathrm{V}$. The frequency of the drive is swept between $100\,\mathrm{Hz}$ and $100\,\mathrm{kHz}$, and the interferometer signal, demodulated at the drive frequency, is squared. This method is similar to the measurement already shown in Figure 4.7. The resulting transfer function, normalized to one at low frequencies, is given in Figure 4.9. The blue points are the results from the sweep, while the red line is a fit with the theoretical transfer function. The resonances at frequencies above $10\,\mathrm{kHz}$ are caused by other vibrational modes of the nested resonator.

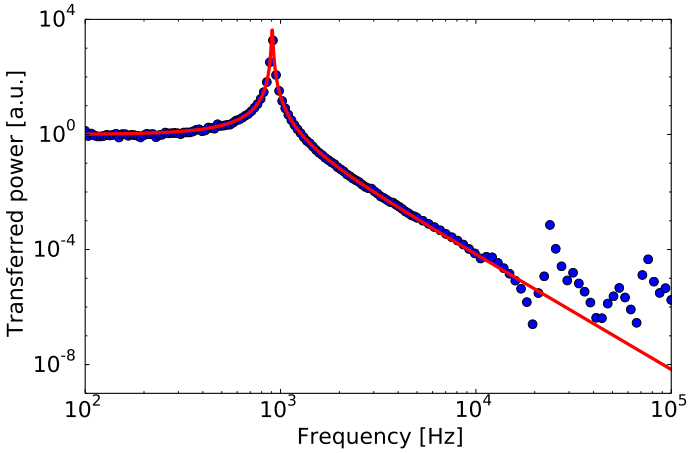

Figure 4.9: Frequency scan of the outer resonator motion (blue dots), converted to the power transferred by the outer resonator. This indicates the amount of vibrational isolation provided by the outer resonator. From the fit to the expected transfer function (red line) we can deduce an isolation of $40\,\mathrm{dB/decade}$, resulting in an expected isolation of $80\,\mathrm{dB}$ at the inner resonance frequency of around $300\,\mathrm{kHz}$.

From the slope of the transfer function above resonance we can infer a mechanical isolation of $40\,\mathrm{dB/decade}$. Since the resonance frequency of the outer resonator is designed to be two orders of magnitude below that of the inner resonator, the mechanical isolation at the inner resonator frequency is expected to be $80\,\mathrm{dB}$. Because of this large isolation, the motion of the resonator at the inner resonator frequency was no longer distinguishable with the sensitivity of the fiber interferometer, so the $80\,\mathrm{dB}$ of isolation could not be measured directly. It is clear, however, that the outer resonator provides significant isolation.

4.3.2 Dielectric force control of the resonator motion

An electric field induces polarization in a dielectric material. The formed dipoles are then attracted towards the point of maximum field strength. If the electric field is homogeneous, the dipoles are attracted equally to the positive and negative electrode and the net effect is zero. In order to create a force to attract the resonator, a strong gradient in the electric field is needed. If we describe the whole dielectric by a single dipole $\mathbf{p}$, the force on it is given by [95]:

$$\mathbf{F}_d = (\mathbf{p} \cdot \nabla)\mathbf{E}. \tag{4.6}$$

In our system the dielectric is the silicon outer resonator attracted to a $100\,\mu\mathrm{m}$ diameter wire positioned in the vicinity. The other electrode is the copper sample mount located far from the resonator, such that the electric field is strongest near the wire. All the data showed in this section are obtained with this wire in the vicinity. However, it turned out that a wire pulls unevenly on the resonator, so in later designs we replaced the wire by a ring electrode with a diameter of $600\,\mu\mathrm{m}$. The relative positions of the ring electrode, SM fiber and nested resonator are indicated in Figure 4.10. The dotted lines represent the electric field lines between the ring electrode and sample mount.

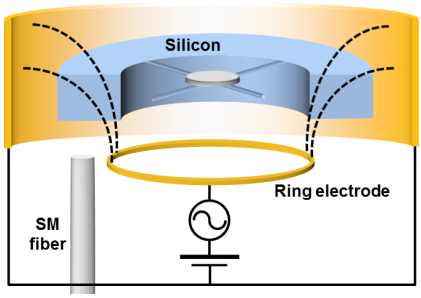

Figure 4.10: Schematic of the the nested resonator surrounded by the sample mount which is electrically connected to a ring electrode positioned near the outer resonator. A single mode (SM) fiber points towards the outer resonator for read-out of its motion. The electric field lines between the ring electrode and sample mount are indicated by the dotted lines.

If we set the direction of the field lines near the ring electrode and through the resonator in the z-direction and ignore the contribution of other directions, the force is equal to

$$F_{d,z} = \varepsilon_0 \chi_e E_z \frac{\partial E_z}{\partial z}, \tag{4.7}$$

with the outer resonator polarized in the z-direction, $p_z = \varepsilon_0 \chi_e E_z$ with χ_e the electric susceptibility of the silicon. The electric field distribution is not trivial and we are ultimately not interested in the exact magnitude of the force. So we further simplify the expression above by observing that the electric field (and its derivative) between the two electrodes is proportional to the applied voltage. It follows that the force depends quadratically on the voltage, just as in the case of a capacitative drive. We can therefore repeat the measurements presented in the previous section by applying similar voltages, namely the sum of a DC voltage to polarize the outer resonator and an AC modulation to influence its motion. The force is then proportional to

$$F_{d,z} \propto [V_{\mathrm{DC}} + V_{\mathrm{AC}} \cos(\omega t)]^2 = \left(V_{\mathrm{DC}}^2 + \frac{1}{2} V_{\mathrm{AC}}^2\right) + 2 V_{\mathrm{DC}} V_{\mathrm{AC}} \cos(\omega t) + \frac{1}{2} V_{\mathrm{AC}}^2 \cos(2\omega t). \tag{4.8}$$

Similar to the result in Figure 4.7 we first check that we can drive the outer resonator by sweeping the AC voltage across the outer resonator frequency, while demodulating the interferometric read-out signal at the same frequency as the drive. Significantly higher voltages are needed than with the capacitative drive: the DC voltage is set to $-40\,\mathrm{V}$ and the AC amplitude is $8\,\mathrm{V}$. Again, the driven motion in Figure 4.11 is compared to the undriven thermal motion obtained from a Fourier transform of the interferometer signal.

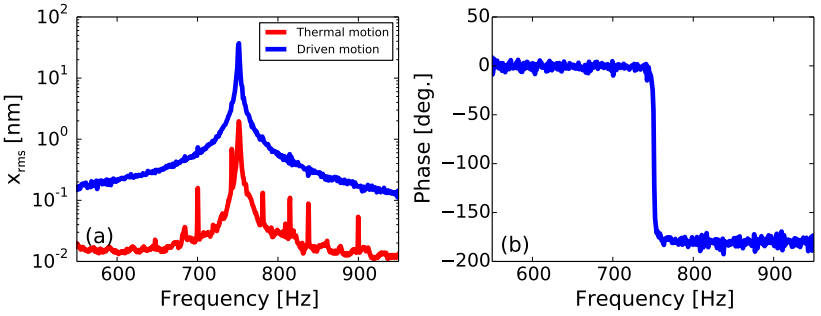

Figure 4.11: Frequency scan of the response of the outer resonator to the dielectric force: (a) Amplitude of the resonator motion (blue line) compared to the undriven thermal motion (red line); (b) Phase of the driven resonator motion.

The outer resonator clearly reacts to the dielectric force, its amplitude increases by more than an order of magnitude. This is a similar response to that observed with the capacitative drive. However, the sample preparation is more convenient, since it only requires positioning a SM fiber and an electrode in the vicinity of the outer resonator. Another disadvantage of the capacitative control was the presence

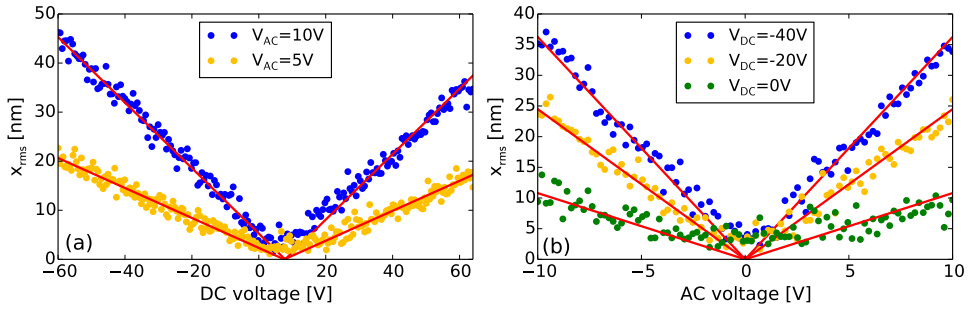

Figure 4.12: Sweeps of the (a) DC and (b) AC voltage while monitoring the response at the applied frequency. The red lines are fits of the expected response through the data points.

of spurious capacitors, influencing the linear response of the resonator on the voltage sweeps in Figure 4.8. These sweeps are repeated in Figure 4.12 with the dielectric drive. The response is now clearly linear, which means that the dielectric force as described by Eq. 4.7 is the only source that drives the resonator and that we can safely create a feedback loop that minimizes the resonator motion without being affected by other effects.

In such a feedback loop the phase-shifted interferometer signal is send back to the positive electrode with an adjustable gain. If the feedback is set correctly, the damping rate of the outer resonator should increase with loop gain. This is verified via amplitude ring-down measurements, where the resonator was first driven to a certain high amplitude before the feedback was switched on. The amplitude of

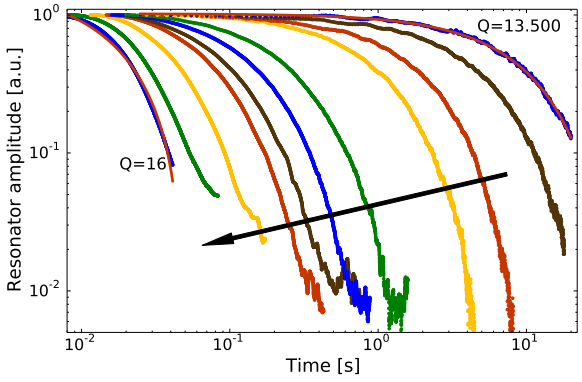

Figure 4.13: Resonator amplitude ring-down measurements with different loop gain. The arrow indicates the direction of increasing gain and, related, increasing damping rate of the outer resonator. From exponential decay fits (red lines, only shown for the outermost ring-downs) the mechanical quality factor is determined.

the outer resonator was measured as a function of time and followed an exponential decay. The quality factor is determined from the time constant. The ring-down measurements are displayed in Figure 4.13 for different values of the loop gain, with increasing gain indicated by the arrow.

With this method, the quality factor of the outer resonator is decreased significantly. Figure 4.13 shows that the quality factor, which starts at 13.500 without feedback, can be reduced to 16. This helps significantly in controlling the outer resonator motion. Even when external vibrations drive the outer resonator, which is likely to happen when the system is placed in a cryostat, this damping system is capable of damping the resonator motion to manageable amplitudes.

4.4 Conclusions and outlook

Adding a resonator around the original trampoline resonator is a good solution to prevent high-frequency vibrational noise from coupling to the trampoline resonator motion. As the single resonator is cooled optically, its signal becomes concealed by these vibrational noise peaks, which limits the achievable observable optical cooling factor. With the nested resonator, the resonator can be cooled further, reaching an effective temperature of 23 mK from room temperature before the signal disappears under the measurement noise floor.

But adding the outer resonator is not solely beneficial. Its mechanical properties influence the stability of the system, making it very sensitive to low-frequency vibrational noise. To damp this motion, two methods of applying a force were investigated: capacitively and dielectrically. Both methods are successful in driving the outer resonator motion and can also be used to damp it. However, using the dielectric force profits from an easier set-up design.

With our control of the outer resonator motion, we have added the possibility to not only lock the laser frequency to follow changes in the cavity length, but also to adjust the cavity length to follow the laser frequency [96]. Instead of letting the laser be influenced by the vibrational noise, the length variations are now eliminated by actively stabilizing the position of the nested resonator.

The mechanical quality factor determines the optical cooling factor that can be achieved before the signal disappears in the background. With the current optical cooling factor, it should in principle be possible to achieve a phonon occupancy of less than one starting at a base temperature of 100 mK. Placing the set-up in a dilution refrigerator is therefore the next logical step.